

## Interfacial role in room-temperature diffusion of Au into Si substrates

J. K. Bal and S. Hazra\*

*Surface Physics Division, Saha Institute of Nuclear Physics, 1/AF Bidhannagar, Kolkata 700064, India*

(Received 17 November 2006; revised manuscript received 8 February 2007; published 8 May 2007)

X-ray reflectivity is used in tracking the diffusion of Au into Si(001) substrates with time at room temperature. It has been observed that the diffusion of Au into Si substrates strongly depends on the initial pretreatment conditions of Si surface. In particular, there is very little diffusion for the untreated Si surface, while the Si surface pretreated with HF seems to be prone to strong diffusion and the surface further pretreated with Br shows diffusion in between. Such different diffusion and apparent non-Fickian-type time dependence in the diffusion can be quantitatively explained by Fickian diffusion of Au through changing unblocked interfacial layer. The growth of the blocking (oxide) layer with time essentially prevents further diffusion through those areas, and the growth of that layer is directly related to the surface stability due to the surface pretreatment and/or passivation conditions, which gives a control in the formation of diffusion-induced Au-Si nanolayer of different widths and compositions. The morphology and evolution of the top surface, mapped with atomic force microscopy and scanning electron microscopy, further helped to verify and understand such differences.

DOI: [10.1103/PhysRevB.75.205411](https://doi.org/10.1103/PhysRevB.75.205411)

PACS number(s): 66.30.Pa, 68.35.Fx, 61.10.Kw, 68.37.Ps

### I. INTRODUCTION

The study of diffusion of Au into Si substrate has long-standing interest in device fabrications.<sup>1</sup> Extensive work has been carried out at elevated temperatures,<sup>2,3</sup> mainly to enhance the diffusion, from which diffusion dynamics in the micron length scale is well established.<sup>4–6</sup> Also, a lot of work is on going to understand the role of surface binding and surface structure in the diffusion process. It is known that the presence of a native-oxide layer or the growth of an oxide layer<sup>7,8</sup> at the interface strongly influences the interdiffusion behavior across a metal-semiconductor interface.<sup>9,10</sup> It is also known that the oxide growth on Si surface could be hindered under non-UHV conditions by passivating the surface dangling bonds. It has been shown that bromine passivates the dangling bonds of the Si(111) surface and this passivated structure is stable for several days in dry air,<sup>11,12</sup> while the bromine passivated Si(001) surface is not so stable.<sup>13</sup> The stability of Si surface after passivation with other material is again different.<sup>13</sup> All these suggest that by controlling the passivation, diffusion of Au into Si can be controlled, which can also be used in the formation of control interdiffused layer. However, not much work has been carried out in this direction to study the initial interfacial role in the formation of thin Au-Si diffuse layer at room temperature, which is of immense interest not only to produce control diffused junctions in silicon at very shallow depth from the surface for the newly developed devices but also for the understanding of the morphological stability of the grown low-dimensional structures due to the diffusion even at room temperature.<sup>14–17</sup> It is now evident that by using nondestructive x-ray reflectivity (XRR) technique,<sup>18,19</sup> growth of very thin interdiffused layer can be well studied;<sup>20,21</sup> this technique essentially provides an electron-density profile (EDP), i.e., in-plane ( $x$ - $y$ ) average electron density as a function of depth ( $z$ ) in high resolution. From the electron density ( $\rho$ ), it is then possible to estimate the mass density ( $\rho_m$ , as  $\rho_m$  is proportional to  $\rho$  for single material<sup>22</sup>) and the diffuse amount.

Here we have utilized this XRR technique to study the time evolution of Au-Si interdiffused layer at room tempera-

ture for differently pretreated Si surface. Our analysis suggests that the growth of a blocking layer (presumably, an oxide layer) at the Au-Si interface prevents further diffusion of Au into Si and, as a result, shows deviation from Fickian-type diffusion. The growth rate of this blocking layer is different for differently pretreated Si surface, which gives rise to a control in the formation of Au-Si interdiffused layer. An attempt has been made to correlate the topography, mapped preliminary by scanning electron microscopy (SEM) and thoroughly by atomic force microscopy (AFM),<sup>22–24</sup> with the observed interdiffusion.

### II. EXPERIMENT

Au films of thickness about 8.5 nm were deposited on Si(001) substrates using magnetron sputtering technique (PLS 500, Pfeiffer) at 25 W power and  $3.5 \times 10^{-3}$  mbar argon pressure for 2 min. Prior to Au deposition, Si substrates (each of about  $10 \times 10$  mm<sup>2</sup> size) were treated differently. The first set of substrates, labeled as OSi, was sonicated in the presence of trichloroethelene (for about 10 min) and methyl alcohol (for about 10 min) separately to remove organic contaminants only, preserving the native-oxide layer on the surface. The second set of substrates, after removal of organic contaminants, was etched with 10% HF solution (for about 3 min) to remove the native-oxide layer and was labeled HSi. The last set of substrates was passivated with Br using bromine (0.05% by volume)-methanol solution (rinsed thoroughly for about 20 min) after the removal of the native-oxide layer and was labeled BrSi. Au was then deposited simultaneously on those three sets of substrates (to get the same thickness) and, correspondingly, they were labeled as Au-OSi, Au-HSi, and Au-BrSi.

XRR measurements of differently pretreated Si substrates as well as Au deposited films were carried out using a versatile x-ray diffractometer (VXRD) setup.<sup>25</sup> VXRD consists of a diffractometer (D8 Discover, Bruker AXS) with Cu source (sealed tube) followed by a Göbel mirror to select and enhance Cu  $K\alpha$  radiation ( $\lambda = 1.54$  Å). The diffractometer

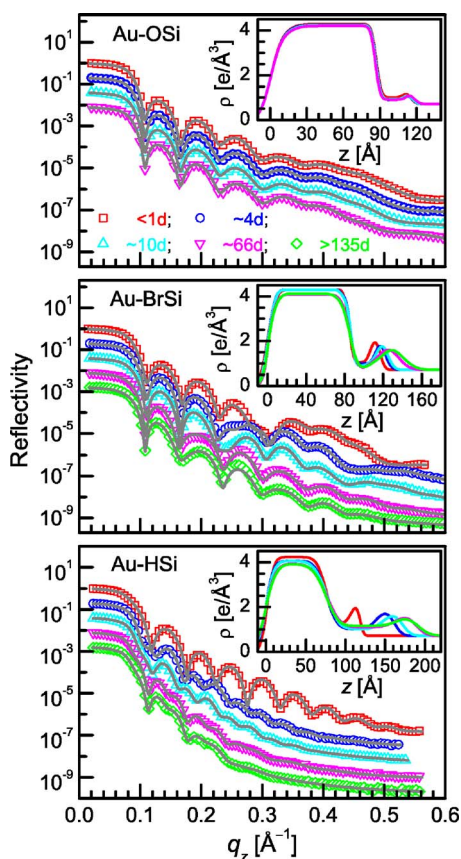


FIG. 1. (Color online) Time evolution XRR data (symbol) and analyzed curves (solid line) of Au thin films on three differently pretreated Si substrates in three panels. In each panel, curves are shifted vertically for clarity. Inset: corresponding analyzed EDP. In legends, d indicates the time in day.

has a two-circle goniometer  $[\theta(\omega) - 2\theta]$  with quarter-circle Eulerian cradle as sample stage. The latter has two circular ( $\chi$  and  $\phi$ ) and three translational ( $X$ ,  $Y$ , and  $Z$ ) motions. Scattered beam was detected using NaI scintillation (point) detector. Data were taken in the specular condition, i.e., the incident angle ( $\theta$ ) is equal to the exit angle ( $\theta$ ) and both are in the scattering plane. Under such condition, a nonvanishing wave vector component,  $q_z$ , is given by  $(4\pi/\lambda)\sin\theta$  and the resolution of the x-ray reflectivity measurements was  $0.0014 \text{ \AA}^{-1}$ . X-ray reflectivity measurements of the Au deposited films were carried out as a function of time to see the interfacial evolution due to diffusion.

Large-scale near-top surface features of the Au films on differently pretreated Si substrates, evolved after prolonged diffusion at room temperature, were first imaged by SEM (Quanta 200 FEG). The detailed top surface morphology of the same films were then mapped through AFM (beam-deflection AFM, Omicron NanoTechnology) in different length scales (50–1000 nm) and in different portions of the samples. AFM images were collected in noncontact mode and in UHV ( $10^{-9}$  mbar) conditions to get less disturbed and clean images, respectively. In the following, we will mainly concentrate on one sample from each set, for which the complete measurements have been carried out.

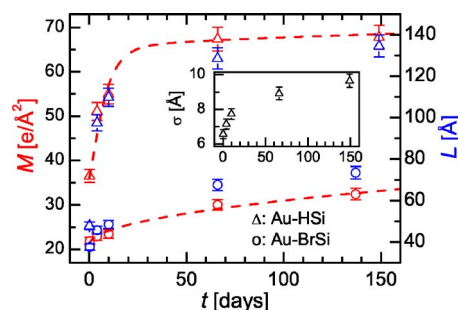


FIG. 2. (Color online) The diffused amount ( $M$ ) and the diffusion length ( $L$ ) of Au in the differently pretreated Si substrates as a function of time. Dashed lines through  $M$  data are the analyzed curves using Eq. (2). Inset: evolution of the surface roughness ( $\sigma$ ) with time for the Au-HSi sample. An error bar has been incorporated for each data.

### III. RESULTS AND DISCUSSION

#### A. Interdiffused layer

The evolution of the interfacial region with time, due to the diffusion of Au into Si through the pretreated surface, can be predicted from the XRR data, which have been presented first, followed by the analysis. The time-dependent diffusion behavior is then predicted from the interdiffused layer estimated from the analyzed EDP.

##### 1. X-ray reflectivity and electron-density profile

Time evolution XRR data of three Au thin films deposited on Si substrates are shown in Fig. 1. Kiessig fringes are evident in all the films, which are the signature of the total film thickness. Along with the Kiessig fringes, a modulation is also observed in the XRR profiles. Such modulation and their evolution with time are different for the films deposited on differently pretreated Si substrates. By monitoring the Kiessig fringes and the modulation, one can readily get an idea about the changes in the film with time. There is very little change in the overall XRR profile of the Au-OSi sample with time, which indicates that the film structure, especially the Au-Si interface structure of this sample, is stable, while changes in the reflectivity curves with time for the Au-BrSi sample are slightly more obvious and that for the Au-HSi sample are significant. These give initial indication of large change in the Au-HSi sample with time.

To get a quantitative information about the samples, all XRR profiles have been analyzed using Parratt's formalism.<sup>26</sup> For the analysis, each film has been divided into a number of layers and roughness has been incorporated at each interface.<sup>22</sup> The thickness, electron density, and roughness associated with each layer were then set as fitting parameters. Best fit XRR profile along with the corresponding EDP are shown in Fig. 1. It is evident from the EDPs that all samples can be visualized as the composition of three regions, namely, top Au layer, interdiffused Au-Si layer, and unmodified Si substrate. The thickness of the top layer ( $d$ ) of each film remains almost the same with time, while that of the interdiffused layer ( $L$ ) is different for different samples. The change in the interdiffused layer is compensated by the

TABLE I. Parameters, such as the thickness ( $d$ ), the electron density ( $\rho$ ), and the top surface roughness ( $\sigma$ ) of the Au thin films; the thickness ( $L$ ) of the interdiffused layer and the decay time ( $\tau$ ), its distribution ( $\beta$ ), and the fraction ( $f$ ) of the active area through which diffusion takes place, for Au thin films on differently pretreated Si substrates obtained from the analysis of the time evolution x-ray reflectivity data. Subscripts  $i$  and  $f$  represent parameters corresponding to the initial and final time of measurements, respectively.

| Sample  | $d$<br>(nm)   | $\rho_i$<br>( $e/\text{\AA}^3$ ) | $\rho_f$<br>( $e/\text{\AA}^3$ ) | $\sigma_i$<br>(nm) | $\sigma_f$<br>(nm) | $L_i$<br>(nm) | $L_f$<br>(nm) | $\tau$<br>(days) | $\beta$ | $f$              |
|---------|---------------|----------------------------------|----------------------------------|--------------------|--------------------|---------------|---------------|------------------|---------|------------------|
| Au-OSi  | $8.7 \pm 0.2$ | $4.28 \pm 0.01$                  | $4.20 \pm 0.01$                  | 0.73               | 0.73               | 3.4           | 3.7           | 0.0 <sup>a</sup> |         | 1.0 <sup>a</sup> |
| Au-BrSi | $8.7 \pm 0.2$ | $4.29 \pm 0.01$                  | $4.12 \pm 0.01$                  | 0.68               | 0.71               | 3.8           | 7.4           | $0.2 \pm 0.1$    | 0.9     | $0.8 \pm 0.08$   |
| Au-HSi  | $8.0 \pm 0.2$ | $4.24 \pm 0.01$                  | $3.92 \pm 0.01$                  | 0.65               | 0.96               | 4.8           | 13.5          | $4.5 \pm 0.5$    | 0.9     | $0.9 \pm 0.05$   |

<sup>a</sup>Nearly covered oxide layer in this Si surface is present from the beginning.

change in the electron density ( $\rho$ ) and/or surface roughness ( $\sigma$ ) of the top Au layer. The parameters obtained from the reflectivity analysis are listed in Table I, where subscripts  $i$  and  $f$  represent parameters corresponding to the initial and final time of measurements, respectively. It can be noted from the EDP that, for the Au-OSi sample, there is very small diffusion of Au at the beginning, which is likely to be through the porous oxide region (the slightly low electron density of the oxide layer usually observed raised the possibility), and then remains almost unchanged ( $L$  changes from 3.4 to 3.7 nm). For the Au-BrSi sample, the diffusion is more evident ( $L$  changes from 3.8 to 7.4 nm) compared to that for the Au-OSi sample, while for the Au-HSi sample, the diffusion seems to be appreciable ( $L$  changes from 4.8 to 13.5 nm).

## 2. Time dependence

In order to understand the time-dependent diffusion of Au, the diffused amount ( $M$ ) has been calculated from the interdiffused layer, subtracting the Si contribution. Parameters  $M$  and  $L$  are then plotted as a function of time ( $t$ ) in Fig. 2 for the Au-BrSi and Au-HSi samples. Similar type of time dependence is observed for both parameters. It is known that for random symmetric diffusion, the diffused amount follows

$$M(t) = M_0 + \Delta M t^{1/2}, \quad (1)$$

where  $M_0$  and  $\Delta M$  are time-independent constants. Strong deviation from the Fickian  $t^{1/2}$  dependence is observed in Fig. 2 for  $M$ . This dependency becomes gradually weaker with time, which is similar to that of jamming or entanglement effect as observed in soft materials (such as polymer) for asymmetric diffusion.<sup>27–29</sup> Such asymmetric diffusion is quite unlikely in our present system, while it is likely that due to the instability of the passivated Si surface some layer (presumably oxide layer) will grow with time through which further diffusion will be blocked. This essentially means that  $\Delta M \propto D$ , where  $D = D_0 e^{-E/kT}$  is not independent of time. The dependency has been incorporated in the following way. First, we have divided the interfacial area into two fractions:  $f$ , where oxide will grow with time, and the rest,  $(1-f)$ , where oxide will never grow; that is, where Si surface will remain passivated. The contribution from  $(1-f)$  fraction is simple Fickian type through constant area, while that from  $f$  fraction changes continuously. If we assume that due to the growth of this oxide layer, the active area, through which

diffusion takes place, decreases exponentially as  $e^{-(t/\tau)^\beta}$ , then the contribution needs to be calculated by considering the average effective area responsible for diffusion up to a certain time, that is, through integration. The diffused amount, in total, can be expressed as

$$M(t) = M_0 + \Delta M' \left[ f \int_0^t e^{-(t'/\tau)^\beta} t'^{1/2} dt' + (1-f)t^{1/2} \right], \quad (2)$$

where  $\Delta M'$  is now a time-independent constant,  $\tau$  is a measure of growth time of the blocking layer, which is also related to the stability of the passivated surface, and  $\beta$  is a stretched exponent.  $\beta$  becomes 1 for single growth time, while deviation from 1 indicates the distribution of growth time. It can be noted here that Eq. (2) is quite general in the sense that for  $f=0$ , it becomes Fickian-type diffusion, while it can be used equally well for  $f=1$  when all the interface acts as a blocking layer. Also, it gives good insight about the growth of the blocking (oxide) layer through  $\tau$ .

Equation (2) has been used to analyze the time-dependent  $M$  for the Au-BrSi and Au-HSi samples. The analyzed curves are shown in Fig. 2 and the corresponding parameters are listed in Table I. It can be noted that for both samples, the

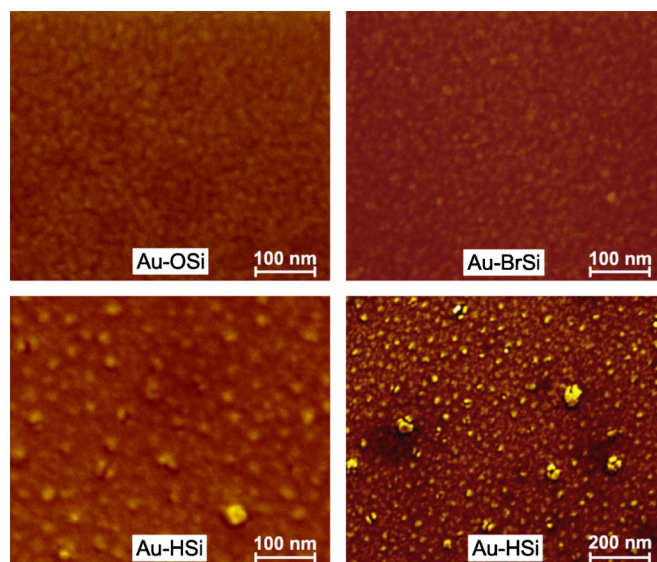


FIG. 3. (Color online) SEM images of Au thin films on differently pretreated Si substrates after prolonged diffusion.

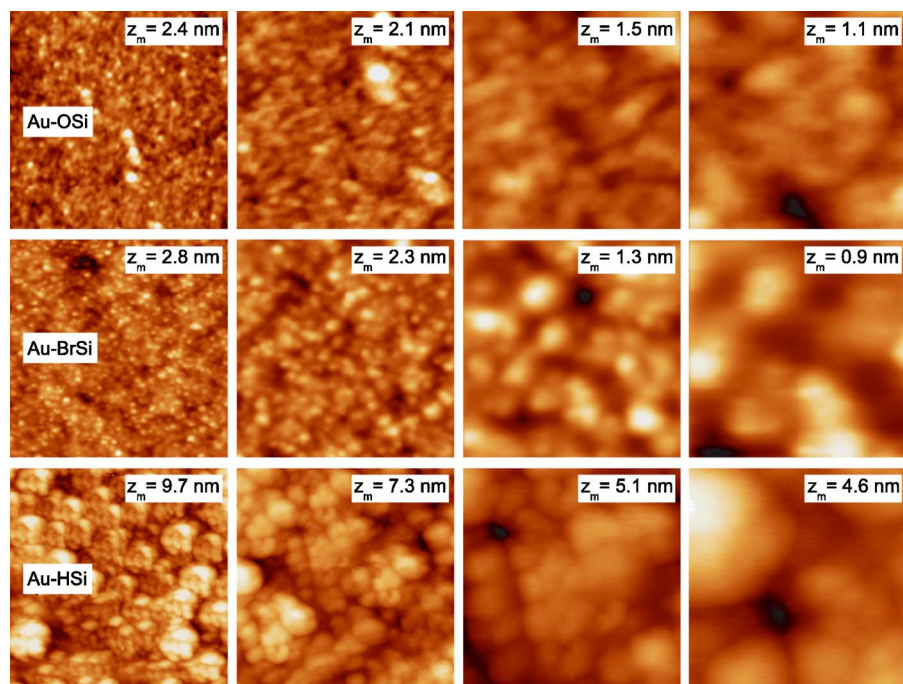


FIG. 4. (Color online) AFM images of Au thin films on differently pretreated Si substrates after prolonged diffusion, in four length scales (1000, 500, 200, and 100 nm from left to right). Maximum height variation is indicated by  $z_m$ .

blocking layer grows in the major portion (large  $f$  value) of the Si surface. Also, for both samples, small but similar distribution ( $\beta=0.9$ ) of  $\tau$  exists. The value of  $\tau$ , on the other hand, differs considerably. Even though a large error is possible in the estimation of  $\tau$ , there is no doubt that  $\tau_{\text{Au-OSi}} \ll \tau_{\text{Au-BrSi}} \ll \tau_{\text{Au-HSi}}$ ; that is, the strong role of surface pretreatment conditions in the growth of the blocking layer even in the presence of Au at room temperature. Large value of  $\tau$ , for the Au-HSi sample, indicates that the Si surface for this sample remains passivated for a longer time, for which large diffusion takes place. It is quite evident that the changes in the density (which is proportional to the electron density) of the Au film and the top surface roughness are due to this diffusion. The variation of the top surface roughness with time is presented in the inset of Fig. 2, which shows a monotonic increase similar to that of the mass diffusion.

### B. Topography

So far, we have discussed the time evolution of the density profiles, which provide changes in the interfacial region due to diffusion. Now, we will present SEM and AFM results and discuss about the topography after diffusion.

#### 1. Scanning electron microscopy

SEM images of three Au thin films, after prolonged diffusion, are shown in Fig. 3. Compact domainlike features

have been observed in all sample surfaces. However, for the Au-OSi and Au-BrSi samples, the contrast is low, while for the Au-HSi sample, the contrast is strong, which is also evident from the additional low magnification image presented in Fig. 3. Considering a single material (Au), such contrast can be primarily associated with the topography and, correspondingly, it can be inferred that the height variation of the surface of the first two samples is quite less compared to that of the latter one. The height variation has been verified by actual topography measurements through AFM, as will be discussed in the next section.

#### 2. Atomic force microscopy and height-height correlation

The AFM images of the same Au thin films are shown in Fig. 4. Domainlike structures of similar size ( $R_D$ ) are evident on the top surface, which is the basic nature of the Au film growth on Si surface.<sup>30</sup> However, the height variation ( $h_{pv}$ ) is different in different films, which is listed in Table II along with  $R_D$ . Height fluctuation of the Au-HSi sample is very high compared to other samples, which can be associated with the fluctuation between accumulated domains due to large diffusion.

A surface can be analyzed quantitatively by height-height (difference) correlation function of the following form:<sup>30-32</sup>

TABLE II. Parameters, such as the domain size ( $R_D$ ), the surface height variation ( $h_{pv}$ ), the saturation surface roughness ( $\sigma_0$ ), the correlation length ( $\xi$ ), and the scaling exponent ( $\alpha$ ), of the Au thin films on differently pretreated Si substrates obtained from the analysis of the AFM images.

| Sample  | $h_{pv}$<br>(nm) | $\sigma_0$<br>(nm) | $R_D$<br>(nm) | $\xi$<br>(nm) | $\alpha$ |
|---------|------------------|--------------------|---------------|---------------|----------|
| Au-OSi  | $2.4 \pm 0.2$    | 0.21               | $25 \pm 4$    | $26 \pm 3$    | 0.86     |
| Au-BrSi | $2.8 \pm 0.2$    | 0.30               | $25 \pm 3$    | $25 \pm 3$    | 0.91     |
| Au-HSi  | $9.8 \pm 0.3$    | 2.00               | $27 \pm 4$    | $40 \pm 4$    | 0.91     |

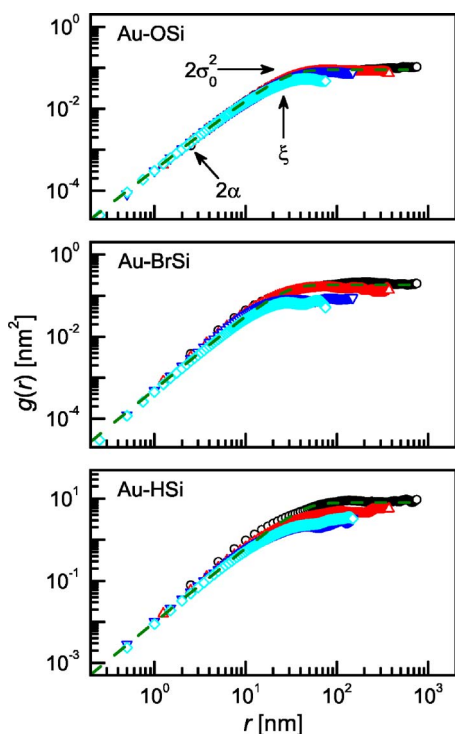


FIG. 5. (Color online) Height-height correlation obtained from AFM images of Au films on differently pretreated Si substrates after prolonged diffusion in different panels. The symbols represent the data estimated from AFM images of different scan sizes, while the dashed lines are the fits corresponding to Eq. (4). Different parameters associated with the height-height correlation function are indicated by arrows for clarity.

$$g(r) = \langle [h(r_0 + r) - h(r_0)]^2 \rangle, \quad (3)$$

where  $h(r_0 + r)$  is the height of the surface at relative position  $r$  and  $h(r_0)$  is the mean surface height. Equation (3) has been used to calculate statistically meaningful  $g(r)$  from the AFM images. Nearly linear increase up to a certain length scale followed by saturation is observed in all the curves. The length scale where the bending is observed, the slope, and the saturation value are the measures of the surface and need to be estimated quantitatively.

It is known that the height-height correlation function, for the kinetic rough surface, follows<sup>30,31</sup>

$$g(r) = 2\sigma_0^2 [1 - e^{-(r/\xi)^{2\alpha}}], \quad (4)$$

where  $\sigma_0$  is the saturation roughness,  $\xi$  is the correlation length, and  $\alpha$  is the scaling exponent of the surface. The height-height correlation data of the different modified surfaces have been fitted using Eq. (4) and are presented in Fig. 5. The different parameters obtained from the analysis are listed in Table II. It can be noted that the scaling exponent is quite high ( $\alpha \sim 0.9$ ) and similar for all the films even after diffusion for a prolonged time, indicative of in-plane diffusion dominated growth as has been observed before in the initial stage.<sup>30</sup> On the other hand, the values of other parameters listed in Table II for the Au-HSi sample are large compared to other samples. This can be understood in the follow-

ing way. In the Au-HSi sample, there are some portions (channels) regularly distributed from where the entire Au layer has been diffused. The distribution of channels is reflected in  $\xi$  value, while the fact that almost the entire layer has been diffused in some portion is reflected in the values of  $h_{pv}$  and  $\sigma_0$ . It can also be noted that the value of  $\sigma_0$  of this film is quite high when compared to the value of  $\sigma_f$  of Table I. This is because of those channels in the film, which mostly appear as a decrease in the electron density in the x-ray reflectivity data analysis, while appearing as high roughness in the AFM measurements due to the convolution with the tip.

### C. Control mechanism

Let us now try to understand the reason behind the observed difference in the diffused amount of Au in three samples and the mechanism for the formation of a controlled interdiffused layer. For the Au-OSi sample, a native-oxide layer was present from the beginning, which prevents Au diffusion into Si. The very small amount of Au that is observed inside Si is diffused through the pores, which are likely to be present in the oxide layer. For the Au-HSi sample, the initial oxide layer of the Si surface was etched off by HF and the surface is supposed to be passivated with H. It is known that the Si surface passivated with H is not stable, and the oxide layer tried to grow with time. To overcome that, Si surface was further passivated with Br in the Au-BrSi sample. However, it has been observed that the surface passivated with Br is less stable compared to that passivated with H only. Although it is apparently surprising, it is known that for Si(001) surface, there are two dangling bonds on each Si atom which need to be saturated.<sup>11</sup> For Br passivation, two Br atoms try to saturate two adjacent dangling bonds of a Si atom, inclined toward each other. However, the size of the Br atom is big such that it is difficult to accommodate both Br atoms in adjacent positions, which makes such a structure unstable. On the other hand, for the small size of H atom such spacial problem does not arise, which makes the H-passivated Si(001) surface more stable than the Br-passivated Si(001) surface. It is then quite evident that the simple passivation in different ways (as demonstrated here) can tune the growth of the oxide layer on the Si surface even in the presence of a thin Au film, which in turn can control the formation of an interdiffused nanolayer. This, in general, implies that by changing the surface stability, the interdiffusion can be controlled at room temperature. In addition, it seems that the use of different oxygen pressures can control the interdiffusion. Also the structures can be developed through interdiffusion by passivating the surface heterogeneously. However, the last two ideas need to be verified experimentally.

### IV. CONCLUSION

The diffusion of Au into Si substrate has been studied at room temperature, for Si surface pretreated differently. Time-evolution x-ray reflectivity measurements suggest strong diffusion of Au into Si substrate when surface is pretreated with HF and, subsequently, large variation in the topography.

While Au deposited on Si surface further pretreated with Br shows small diffusion, that on untreated Si surface shows negligible diffusion with relatively smooth topography. The evolution of the Au-Si interdiffused layer with time has been attributed to the diffusion of Au through unblocked Si surface. The unblocked area through which diffusion takes place decreases exponentially with time. The growth of the blocking layer is related to the surface stability due to surface passivation. We claim that by changing the surface passiva-

tion, stability of the surface can be changed, which then can be used to control the layer of interdiffusion in nanometer length scale.

#### ACKNOWLEDGMENTS

The authors would like to thank Srinanda Kundu for her valuable help in magnetron sputter deposition and Souvik Banerjee for his assistance in SEM imaging.

\*Electronic address: satyajit.hazra@saha.ac.in

- <sup>1</sup>C. B. Collins, R. O. Carlson, and C. J. Gallagher, *Phys. Rev.* **105**, 1168 (1957).
- <sup>2</sup>W. R. Wilcox and T. J. LaChapelle, *J. Appl. Phys.* **35**, 240 (1964).
- <sup>3</sup>A. Rodriguez, H. Bracht, and I. Yonenaga, *J. Appl. Phys.* **95**, 7841 (2004).
- <sup>4</sup>F. C. Frank and D. Turnbull, *Phys. Rev.* **104**, 617 (1956).
- <sup>5</sup>U. Gösele and H. Strunk, *Appl. Phys.* **20**, 265 (1979).
- <sup>6</sup>A. V. Vaisleib, M. G. Goldiner, O. Y. Keloglu, and I. N. Kotov, *J. Appl. Phys.* **70**, 6809 (1991).
- <sup>7</sup>L. C. Ciacchi and M. C. Payne, *Phys. Rev. Lett.* **95**, 196101 (2005).
- <sup>8</sup>T. Watanabe, K. Tatsumura, and I. Ohdomari, *Phys. Rev. Lett.* **96**, 196102 (2006).
- <sup>9</sup>A. Cros and P. Muret, *Mater. Sci. Rep.* **8**, 271 (1992).
- <sup>10</sup>L. A. Baker, A. R. Laracuente, and L. J. Whitman, *Phys. Rev. B* **71**, 153302 (2005).
- <sup>11</sup>G. W. Trucks, K. Raghavachari, G. S. Higashi, and Y. J. Chabal, *Phys. Rev. Lett.* **65**, 504 (1990).
- <sup>12</sup>J. F. Chang, T. F. Young, Y. L. Yang, H. Y. Ueng, and T. C. Chang, *Mater. Chem. Phys.* **83**, 199 (2004).
- <sup>13</sup>K. Sekar, P. V. Satyam, G. Kuri, D. P. Mahapatra, and B. N. Dev, *Nucl. Instrum. Methods Phys. Res. B* **71**, 308 (1992).
- <sup>14</sup>H. D. Hallen, A. Fernandez, T. Huang, R. A. Buhrman, and J. Silcox, *J. Vac. Sci. Technol. B* **9**, 585 (1991).
- <sup>15</sup>C. R. Chen and L. J. Chen, *J. Appl. Phys.* **78**, 919 (1995).
- <sup>16</sup>J. H. Kim, G. Yang, S. Yang, and A. H. Weiss, *Surf. Sci.* **475**, 37 (2001).
- <sup>17</sup>V. N. Antonov, J. S. Palmer, P. S. Waggoner, A. S. Bhatti, and J. H. Weaver, *Phys. Rev. B* **70**, 045406 (2004).
- <sup>18</sup>I. K. Robinson and D. J. Tweet, *Rep. Prog. Phys.* **55**, 599 (1992).
- <sup>19</sup>*X-ray and Neutron Reflectivity: Principles and Applications*, edited by J. Daillant and A. Gibaud (Springer, Paris, 1999).
- <sup>20</sup>M. K. Sanyal, S. Hazra, J. K. Basu, and A. Datta, *Phys. Rev. B* **58**, R4258 (1998).
- <sup>21</sup>S. Hazra, S. Chakraborty, and P. T. Lai, *Appl. Phys. Lett.* **85**, 5580 (2004).
- <sup>22</sup>S. Kundu, S. Hazra, S. Banerjee, M. K. Sanyal, S. K. Mandal, S. Chaudhuri, and A. K. Pal, *J. Phys. D* **31**, L73 (1998).
- <sup>23</sup>J. K. Basu, S. Hazra, and M. K. Sanyal, *Phys. Rev. Lett.* **82**, 4675 (1999).
- <sup>24</sup>*Noncontact Atomic Force Microscopy*, edited by S. Morita, R. Wiesendanger, and E. Meyer (Springer, Heidelberg, 2002).
- <sup>25</sup>S. Hazra, *Appl. Surf. Sci.* **253**, 2154 (2006).
- <sup>26</sup>L. G. Parratt, *Phys. Rev.* **95**, 359 (1954).
- <sup>27</sup>D. A. Edwards, *J. Polym. Sci., Part B: Polym. Phys.* **34**, 981 (1996).
- <sup>28</sup>*Jamming and Rheology: Constrained Dynamics on Microscopic and Macroscopic Scales*, edited by A. J. Liu and S. R. Nagel (Taylor & Francis, London, 2001).
- <sup>29</sup>G. Hornung, B. Berkowitz, and N. Barkai, *Phys. Rev. E* **72**, 041916 (2005).
- <sup>30</sup>A.-L. Barabási and H. E. Stanley, *Fractal Concepts in Surface Growth* (Cambridge University Press, Cambridge, 1995).
- <sup>31</sup>S. K. Sinha, E. B. Sirota, S. Garoff, and H. B. Stanley, *Phys. Rev. B* **38**, 2297 (1988).
- <sup>32</sup>F. Family and T. Viscek, *Dynamics of Fractal Surface* (World Scientific, Singapore, 1991).